Inverse Hardening Soil Parameter Identification of an Earth and Rockfill Dam by Genetic Algorithm Optimization

Pooya Vahdati
Department of Civil, Environmental and Natural resources engineering, Luleå University of Technology, Luleå, Sweden
e-mail: Pooya.Vahdati@ltu.se

Dr. Séverine Levasseur
Département ArGEnCo Service de Géomécanique et géologie de l'ingénieur Université de Liège, Liège-Belgium,
e-mail: severine.levasseur@ulg.ac.be

Hans Mattsson
Assistant Professor
Department of Civil, Environmental and Natural resources engineering, Luleå University of Technology, Tel: +46 920 492147, SE – 971 87, Luleå, Sweden
e-mail: Hans.Mattsson@ltu.se

Sven Knutsson
Professor
Department of Civil, Environmental and Natural resources engineering, Luleå University of Technology, Tel: +46 920 491332, SE – 971 87, Luleå, Sweden
e-mail: Sven.Knutsson@ltu.se

ABSTRACT

This paper presents a study of identification of constitutive parameter values in the Hardening soil model by inverse analysis of an earth and rockfill dam application. The authors have experience from a previous study on the same case with the Mohr-Coulomb model. The objective of this research is to examine if the inverse analysis technique can be successfully used for this type of application and choice of constitutive model. The values of soil parameters are determined based on horizontal deformations obtained from installed instrumentations in the dam. The quantities that are monitored in the dam can be numerically predicted by a finite element simulation. In inverse analysis, constitutive parameter values are chosen in such a way that the error between data recorded by measurements in the dam and numerical simulation is minimized. An optimization method based on the genetic algorithm was applied to search for the minimum error in the search domain in this study. Optimizations have initially been performed in a large search domain in order to find a criterion identifying the best solutions. Thereafter, the optimizations were limited to this criterion in order to find the best set of solutions close to the optimum point. Moreover, the error function topology and smoothness was examined as well. It was overall concluded, that the inverse analysis technique could be effectively used for earth and rockfill dam applications, despite the fact that the technique is expensive in terms of computational time.

KEYWORDS: earth and rockfill dam, finite element modelling, inverse analysis, genetic algorithm, Hardening soil model.

INTRODUCTION

Computational modelling of earth and rockfill dams might not be an easy task if limited information is available about the material properties in the dam zones, due to lack of reliable relevant data which is the case for many old dams. In addition, taking samples for testing from dam zones, especially from the core, the central impervious part, is normally very difficult since it might affect the dam performance and the safety.

Inverse analysis can provide a method to determine the constitutive behaviour of various materials within the dam structure if the dam is well equipped with different instrumentations. In the method of inverse analysis, two separate parts are included: (1) an optimization method consisting of an error function and a search algorithm and (2) a numerical method to solve the partial differential equations arising in stress-strain analysis of structures. In this study, the numerical modelling was performed with a commercial finite element program Plaxis (2011) and the genetic algorithm was utilized as the search algorithm in the optimization method. The genetic algorithm was chosen due to its robustness, efficiency and particularly since it provides a set of solutions close to the optimum solution instead of one unique answer; a set of solutions is more practical from a geotechnical perspective. With an inverse modelling approach, a finite element model is calibrated step by step by changing the input values of the constitutive model or models until the difference between the measured data by the dam instrumentations and the associated computed values is minimized. The inverse analysis technique was introduced to the geotechnical field by Gioda and Sakurai (1987) for the purpose of identification of elastic material properties of in situ rock masses. Inverse analysis has been widely used recently thanks to the availability of sufficiently fast computer hardware and useful software. In the geotechnical engineering field the interest of applying inverse parameter identification strategies and optimization algorithms modelling in order to make inverse analysis procedures automated is growing fast (Swoboda et al. 1999, Gioda et al. 1980, Tarantola 2005, Calvello et al. 2002 and 2004, Finno et al. 2005, Ledesma et al. 1996, Lecampion et al. 2005, Lecampion et al. 2002, Zentar et al. 2001, Yu et al. 2007, Moreira et al. 2013, Levasseur et al. 2008, 2009 and 2010, Rechea et al. 2008, Papon et al. 2012).

Soil behavior is very complicated and can vary considerably under different loading conditions. Fundamentally, soil behaves as an elasto-plastic material. No constitutive model can completely describe the complex behavior of different soils in all loading situations. Therefore, constitutive models have limitations to their applicability. All models have certain advantages and limitations which highly depend on their particular application. Accurate modelling of deformation and strength in earth and rockfill dams requires a complex stress-strain model. Duncan (1996) recommends the use of models that incorporate plasticity theory for modelling undrained behavior, e.g. for wet placed earthfill cores of thin to medium width in zoned embankments. From the deformation modelling of a concrete face rockfill dam (CFRD), Kovacevic (1994) draws the conclusion that elasto-plastic constitutive models are more suited to accounting realistically for the rockfill deformation behavior under the stress path conditions imposed. In this research, the constitutive relations of the zones of soil were represented by the Hardening soil model. This model was originally developed from the Duncan-Chang hyperbolic model (Duncan et al. 1970, Duncan 1981). However, this model, by using plasticity theory instead of elasticity theory could overcome the restrictions of hyperbolic models. The Hardening soil model includes dilatant soil behavior and introduces a yield cap. Since in reality the stiffness of soils depends on the stress level, the Hardening soil model is formulated to capture this stress level dependency.

The stress and strain behavior in embankment dams, which is governed by loads, particularly: dead weight of soil layers, water reservoir pressure and seismic activity, is predicted from the strength variation and the deformation behavior of soil under combined stresses. Deformations in embankment dams are due to changes in effective stress during construction, impoundment and reservoir fluctuations. The high horizontal stress from the water load acting on the upstream face of the core results in greater changes in lateral than vertical stress in the core and downstream shoulder. Therefore, the deformations will be significantly in the horizontal direction. The magnitude of the deformations depends on the changes in stress conditions as well as the compressibility and stiffness properties of the core and downstream rockfill. Based on studies of several monitored dams, Hunter (2003) shows that dams with poorly compacted rockfill in the downstream shoulder or embankments with cores of silty sands to silty gravels had great lateral crest displacements due to the reservoir impoundment.

The objective of this paper is to study if the inverse analysis technique can be effectively used for identification of constitutive parameter values in the advanced Hardening soil model, in an earth and rockfill dam application. The robustness and efficiency of the inverse analysis procedure and the genetic algorithm as a search algorithm were examined in a previous study, performed by the authors, based on the Mohr-Coulomb model for a synthetic case, Vahdati et.al (2013). Therefore, in this research it was focused only on the real dam case with the Hardening soil model as the constitutive model. In this study, geometry and zoning as well as inclinometer data from an existing earth and rockfill dam were used, see figure (1).

In this research, the inverse analysis was performed against two situations named case A and B, regarding the reservoir water level and the time for the construction of the berms. Moreover, the topology of the error function surface was studied to obtain knowledge about its shape and how the individual solutions in the optimized set of solutions become distributed on the function surface for the two cases. At the end, a proper range of values for the optimized parameters was defined based on inclinometer data and the associated numerically simulated values. Notice that the optimizations presented in this paper are voluntarily restricted to two optimization variables.

A very good agreement from the best set of solutions was obtained against the inclinometer measurements for both case A and case B. The Hardening soil model captured the pattern of horizontal displacements quite well.

THE EARTH AND ROCKFILL DAM

The earth and rockfill dam used for the case study is 45m high, with a dam crest of 6.5m, see figure (1). The downstream slope is inclining 1V:1.85H and the upstream slope is inclining 1V:1.71H. The impervious core, consisting of moraine materials, is surrounded by fine and coarse filters and a supporting fill of blasted rock. The dam was strengthened in two stages with rockfill berms on the downstream part. The first stabilizing berm of rockfill was constructed in 1990 and the second berm was constructed three years later in 1993. The dam is well equipped with instrumentations and monitoring programs including deformation measurements within the dam structure. Horizontal displacements are measured by an inclinometer installed along the downstream fine filter, from the crest into the rock foundation. Since the inclinometer data from the ten first meters from the bottom of the core seem not to be trustworthy, only data above this level are considered. The level of water in the reservoir annually changed from +430m to +440m.

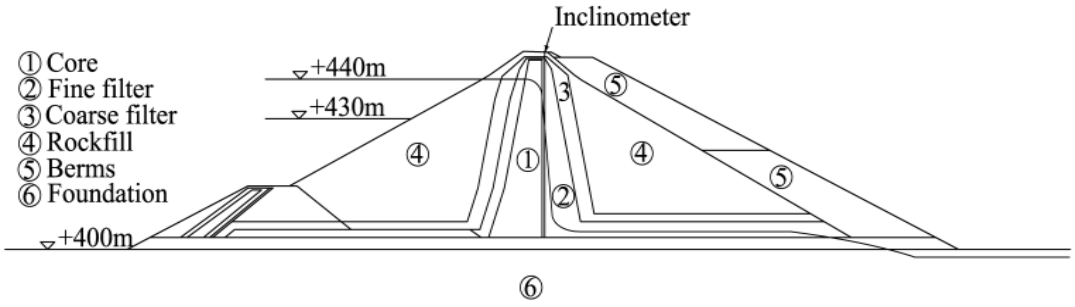

Figure 1: Cross section of the dam

FINITE ELEMENT MODEL

The Plaxis finite element program (2011) was applied to the numerical analyses in this study. The finite element model of the cross section of the dam is shown in figure (2). Because the dam is a long structure, a plane strain model was presumed. Some smaller simplifications compared to the real dam cross section in figure (1) were made in the finite element model in figure (2), e.g. the upstream toe berm was neglected due to similarity in its material properties with rockfill. Horizontal filters were ignored as well, since consolidation time is not taken into account. These simplifications had no practical influence on the modelling of this dam. For the geometry boundary conditions which are provided by fixities in Plaxis, the horizontal displacement of the outermost vertical left and right foundation boundary as well as the horizontal and vertical displacement of the lowest horizontal boundary was prescribed to zero. The finite element mesh type was chosen as 15-noded triangular elements with twelve-Gauss points for the integration. Computation time is an important issue in inverse analysis, so the coarseness of the mesh was selected so that a sufficient accuracy of the computations was obtained for a minimum of computation time spent. Several different meshes were tested and the one showed in figure (2) was chosen. The dam embankment in the model in figure (2) was built up stepwise in five stages in order to generate a proper initial effective stress field (Duncan 1996, Reséndiz et al. 1972, Clough et al. 1967). The excess pore pressures in the core were dissipated by consolidation after construction of the dam. For this study two cases (A and B) based on different reservoir water levels and the number of berms constructed, were analyzed. Case A, refers to the time when the first stabilizing berm was constructed in 1990 and the reservoir water was at the minimum level of +430m. Case B, refers to when the reservoir water level reached its maximum level +440m and the second berm was just finished. The second berm was rapidly constructed right after the water level reached +440m. All the data of horizontal displacements from finite element computations received from exactly the same positions in the geometry as the measurements carried out with the single inclinometer in figure (1) were compared to the related inclinometer measurements in the expression for the error function. In the finite element analysis, all displacements were reset to zero before impoundment.

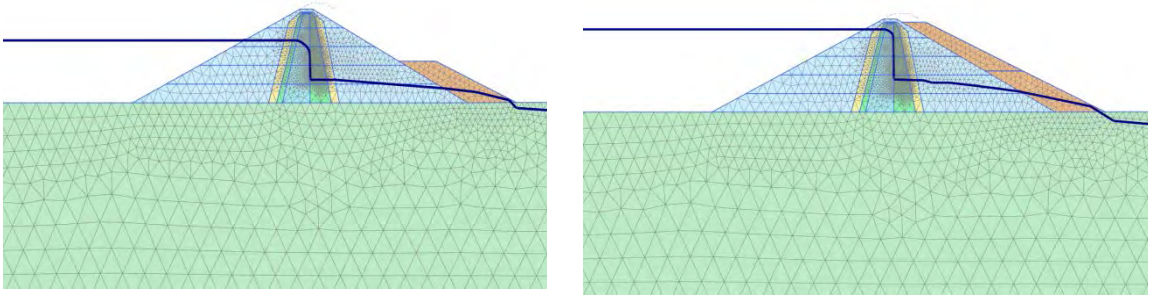

Case A Case B

Figure 2: Finite element model of the dam for case A and case B

CONSTITUTIVE LAW; HARDENING SOIL MODEL

The Hardening soil model is a cone-cap model (Schanz et al. 1999). The plastic strain behavior on the cone is described by means of a shear yield surface following a non-associated flow rule based on Rowe's stress-dilatancy theory (1962). The plastic potential is defined to assure a hyperbolic stress/strain response for triaxial compression loading. The cap yield surface is controlled by the volumetric plastic strain. On this cap, an associated flow rule is assumed. This yield surface is defined in order to close the elastic region in the p'-axis direction, see figure (14). The failure on the cone part is defined based on Mohr-Coulomb's failure criterion which is characterized by the cohesion c', the friction angle ϕ' and the dilatancy angle ψ'. The Hardening soil model use a hyperbolic stress-strain curve on the cone instead of a bi-linear relation as in the Mohr-Coulomb model.

The Hardening soil model has stress-dependent moduli parameters, E_{50} , E_{oed} and E_{ur}, which are defined by a power law parameter m. E_{50} , E_{oed} and E_{ur} are the secant stiffness in primary triaxial loading, tangent (oedometer) stiffness and unloading/reloading stiffness, respectively. These stress dependent moduli E_{50}^{ref}, E_{oed}^{ref} and E_{ur}^{ref} are introduced in Plaxis as parameters associated to a reference pressure (P^{ref}=100 kPa). The power law parameter m controls the shape of the cone-cap yield loci and m is varied from 0.5 for a typical hard soil to 1 for a clay soil. The parameter values of γ_u γ_s, ϕ', k_x and k_y (quantities are explained in table 2) for all soil layers in the dam were provided by the dam owner. Proper values of c' were chosen based on advices in Bowles (1988). All the dilatancy angles were calculated from the same empirical relation, commonly accepted for dense sand: $\psi' = \phi' - 30°$ as proposed by Plaxis (2011). The unloading/reloading Poisson's ratio ν_{ur}, is usually set between 0.15-0.30. Table (1) presents the conventional way of estimating parameters of the Hardening soil model as well as some appropriate default values based on recommendations from Plaxis (2011).

Schanz and Vermeer (1998) showed that based on standard drained triaxial tests the reference secant stiffness E_{50}^{ref} of sand varied from 15 MPa for loose sand to 50 MPa for dense sand. In this study, the filter materials are close to dense sand, therefore the value of E_{50}^{ref} was chosen to 50 MPa for these zones. The range of values for the reference secant stiffness of the core E_{50C}^{ref} and the reference secant stiffness of the rockfill material E_{50R}^{ref} for both case A and case B, were obtained from optimizations against the dam application in this study. A high value of the reference secant stiffness was considered for the foundation to make it rigid. Table (2)

summarizes the values of the material properties of the rockfill dam which are utilized in this case study.

The dam core was modeled with the option of undrained case A in the Plaxis software, an option in which effective strength parameters are utilized. This mode was chosen in order to capture the hardening behavior of the soil. Undrained case B (undrained strength, $\phi' = 0$ and $c' = c_u$) as utilized by the authors Vahdati et.al (2013) in a previous study, is not able to capture the stress dependency behavior in the Hardening soil model and the response would become as in the Mohr-Coulomb model (constant stiffness). All the other dam zones were modeled with the option of drained behavior, i.e. no excess pore pressures are generated.

Table 1: Parameters of the Hardening soil model

Parameter	Definition	Relation
ϕ'	Friction angle	Slope of the failure line in τ - σ' stress plane
$*R_f$	Failure ratio	$R_f = \frac{q_f}{q_a}$
ψ'	Dilatancy angle	$\psi' = \phi' - 30°$
$*E_{50}^{ref}$	Reference secant stiffness for primary loading in a drained triaxial test	$E_{50} = E_{50}^{ref}\left(\frac{c' cot\,\phi' - \sigma_3'}{c' cot\,\phi' - P^{ref}}\right)^m$
$*E_{oed}^{ref}$	Reference tangent stiffness for primary oedometer loading	$E_{oed} = E_{oed}^{ref}\left(\frac{c' cot\,\phi' - \sigma_1'}{c' cot\,\phi' - P^{ref}}\right)^m$
$*E_{ur}^{ref}$	Reference stiffness for unloading\reloading in a drained triaxial test	$E_{ur} = E_{ur}^{ref}\left(\frac{c' cot\,\phi' - \sigma_3'}{c' cot\,\phi' - P^{ref}}\right)^m$
m	Power for stress-level dependency of stiffness	Slope of trend line in $\log\left(\frac{\sigma_3'}{P^{ref}}\right)$ - $\log E_{50}$ plane
$*\nu_{ur}$	Poisson's ratio for loading\unloading	0.15-0.30
K_0	Earth pressure coefficient at rest	$K_0 = \frac{\sigma_3'}{\sigma_1'}$
K_0^{nc}	Earth pressure coefficient value for normally consolidated soil	$K_0^{nc} = 1 - \sin\phi'$

Note: q_f is the ultimate deviatoric stress, q_a is the asymptotic deviatoric stress, P^{ref} is the reference pressure (P^{ref}=100 kPa)

* $E_{50}^{ref} = E_{oed}^{ref}$, $E_{ur}^{ref} = 3E_{50}^{ref}$, $R_f = 0.9$ and $\nu_{ur} = 0.2$ in this study

Table 2: Material properties of the rockfill dam

Dam zones	γ_u	γ_s	$E_{50}^{ref}=E_{oed}^{ref}$	E_{ur}^{ref}	m	c'	ϕ'	k_x/k_y
	kN/m^3		MPa	MPa	-	kPa	(°)	m/s
Core	21	23	70-100	210-300	1	20	38	$3.0\cdot10^{-7}$
Fine filter	21	23	50	150	0.5	0	32	$9.0\cdot10^{-5}$
Coarse filter	21	23	50	150	0.5	0	34	$5.0\cdot10^{-4}$
Rockfill	19	21	10-17	30-51	0.5	7	30	$1.0\cdot10^{-2}$
Berms	21	23	10	30	0.5	7	30	$5.0\cdot10^{-2}$
Foundation	21	23	3000	9000	0.5	0	45	$1.0\cdot10^{-8}$

Note: γ_u is the unit weight above the phreatic level, γ_s is the unit weight below the phreatic level, E_{50}^{ref} is the Reference secant stiffness for primary loading in a drained triaxial test, E_{oed}^{ref} is the Reference tangent stiffness for primary oedometer loading, E_{ur}^{ref} is the Reference stiffness for unloading\reloading in a drained triaxial test, m is the Power for stress-level dependency of stiffness, c' is the effective cohesion, ϕ' is the effective friction angle and k_x and k_y are the hydraulic conductivity in horizontal and vertical direction, respectively.

OPTIMIZATION METHOD

The aim of optimization is to reach the optimum solution among other solutions for a given problem in a matter of efficiency. For any kind of optimization an error function and a search method are needed. In this paper, the error function provides a scalar measure of the discrepancy between horizontal deformations obtained by inclinometer measurements and numerical simulations, respectively. The genetic algorithm was chosen as the search method for the purpose of finding the minimum value of the error function. The variables for optimizing, the selected parameters, are included in constitutive models utilized for the finite element computations. Notice that, the magnitude of the error function is thereby influenced by the values of the optimization variables. The optimal values of the chosen parameters are progressively approached through iteration by minimizing the error function; that is the optimum solution.

ERROR FUNCTION

In order to define the difference between the measured values and finite element computed values, it is necessary to define a proper error function. In this research, following Levasseur et al. (2008) a scalar error function F_{err} based on the least-square method was introduced

$$F_{err} = \left(\frac{1}{N} \sum_{i=1}^{N} \frac{\left(U_{e_i} - U_{n_i}\right)^2}{\Delta U_i^2} \right)^{1/2} \quad (1)$$

That determines the difference between experimentally measured values U_{e_i} and numerically computed values U_{n_i}, from the N measuring points. The term $1/\Delta U_i$ gives the weight of the

difference between U_{e_i} and U_{n_i}. The parameter ΔU_i relates to the numerical and experimental uncertainties at the measurement point *i*; defined as

$$\Delta U_i = \varepsilon + \alpha U_{e_i} \tag{2}$$

where the parameter ε is an absolute error of measurements and the parameter α is a dimensionless relative error of measurements.

In this study the error function defined in equation (1) is considered with the parameters $\varepsilon = 1$ and $\alpha = 0$. That is to say, the function, given by equation (1) is reduced to

$$F_{err} = \left(\frac{1}{N} \sum_{i=1}^{N} \left(U_{e_i} - U_{n_i} \right)^2 \right)^{1/2} \tag{3}$$

and has the unit of length.

SEARCH ALGORITHM

The genetic algorithms were developed originally in the field of artificial intelligence by John Holland in 1970s at the University of Michigan and popularized as a universal optimization algorithm; the method was inspired by Darwin's theory of evolution. The genetic algorithms are computationally and numerically simple and powerful in their search for improvement. The genetic algorithm is a global optimization technique which is based on the genetic mechanisms, such as reproductions, crossings and mutations, with the aim of localizing an optimum set of solutions close to the optimum without being trapped into local optima in the given search domain; but without any guarantee of finding the exact global optimum (Pal et al. 1996, Gallagher et al. 1991, Haupt 1998). Furthermore, this search algorithm is not fundamentally restricted by smoothness properties of the error function surface, like continuity and existence of derivatives. The optimization program that is used in this research was developed in the FORTRAN language by Levasseur et al. (2008, 2009 and 2010) for geotechnical studies.

In the genetic algorithm, the space of search is defined based on the number of parameters N_p to optimize. The minimization problem is approached in the N_p dimensional space limited by the upper and the lower bound constraints of each parameter. The value of each optimization parameter is binary encoded to a form of gene. Each gene is encoded into a part of the bit string in order to be passed to the numerical model. The combination of the genes forms individuals (or chromosomes). An individual is a genetic algorithm chromosome which has raw genetic information Individuals are the single solutions. The population's size N_i consists of the set of individuals, solutions, involved in the search domain. First, an initial population, twice the population size in this study, is defined by random choice of values of chromosomes in N_p domain. The initial population represents the start of the search for the optimum, and explores in the search space spanned by the optimization variables and their boundaries. Initially, these random solutions need to be evaluated. Based on the individual's fitness value, the population is sorted in ascending or descending order. In the genetic algorithm the fitness is the value of the error function for its individual. Only N_i /3 of the best individuals are selected for the next population, which are called parents. Randomly selected pair parents, good temporary solutions, produce a new generation (offspring), which get some parts of the parents' genetic material, based on crossover or mating. The most common form of mating includes two parents that produce two children (offspring). The position of crossover points is randomly chosen and the

value of each binary string exchanges with another one after this position point. Each parent copies e.g. half the gene to each child, with the selection of the gene part being chosen randomly. In order to improve the efficiency of the algorithm a crossover point number is chosen equal to the number of selected parameters, which was proposed by Pal et al. (1996). This process is repeated until $2N_i/3$ children are created. Now the new population, consisting of parents and children is completed. The procedure of selection, crossing and reproduction is called breeding. Mutations apply for preventing the genetic algorithm from converging too fast before sweeping the entire search domain. Mutation is the variation of a randomly selected bit in the parameter code based on a specific probability.

POPULATION SIZE

A proper population size must be chosen before running any genetic algorithm computation. The size of the population must initially be large enough to be effectively spread out over the search space. To avoid a prohibitive CPU time, it is then necessary to dynamically reduce the size of this population (Chelouah et al. 2000). Also, large population sizes would be required to reduce the risk of solutions getting trapped in local optima on the noisy and fluctuated error function surface. However, the drawback of large population sizes is the computation time cost which in some cases could be equivalent to a random search. A small population would be more likely to quickly converge, which might be to a local optima, and the quality of convergence is left to chance. A population sizing equation from statistical theory proposed by Goldberg et al. (1991) and analyzed by Carroll (1996) was studied in this research

$$n_{pop}=m\,X^k=l/_k\,X^k \tag{4}$$

where X is the number of possibilities for each chromosome, e.g. for binary X=2, l is the length of chromosome and k is the size of schema, details about the schema can be found in Goldberg (1989).

To estimate a proper population size, it was considered that each parameter string would represent one schema. So, the length of the schema was assumed to be equal to parameter length for this purpose. For this study, l =12, X=2 and k=6. Therefore the proper population size based on this theory would be

$$n_{pop}=(12/_6)(2^6)=128 \tag{5}$$

The population size which was chosen based on numerical tests in Vahdati et.al (2013), agrees well with results obtained with equation (5).

INVERSE ANALYSIS OF CASE A AND CASE B

This study is a continuation of a previous study, Vahdati et.al (2013), for the purpose of improving the choice of constitutive model from the simple Mohr-Coulomb model to the advanced Hardening soil model to monitor whether it is possible to approach a better agreement with inclinometer data of horizontal displacements. The finite element models of cases A and B are presented in figure (2). In the previous study, only case B was considered with the incremental stiffness theory of the Mohr-Coulomb model. According to available data and results from that study, the smallest average error function value is considered as an upper limit of the error function value for this study, in order to monitor if the advanced Hardening soil model is

able to approach better results compared to the Mohr-Coulomb model. For case A, no former studies were made and an upper limit for the error function value needs to be defined. Therefore, before starting to utilize the Hardening soil model, as the main constitutive model in this research, the upper limit of the error function value for case A should be defined.

MOHR-COULOMB MODEL AND CASE A

In the previous study, it was assumed that the stiffness of soil increase linearly with depth with regards to the weight of soil, a shear modulus increment per unit of depth, G_{inc} was defined for the core, filters and rockfill materials. From the sensitivity analysis, the shear modulus increment of the core G_{inc}^{core} and the shear modulus increment of the rockfill $G_{inc}^{rockfill}$ were the two optimization variables for the inverse analysis based on the Mohr-Coulomb model. Moreover, the population size of 120 was selected as the best population size for the inverse analyses which is also suggested theoretically above. Therefore, based on these assumptions, for the purpose of defining the lowest error function value for case A, initially, ten inverse analyses were performed in a search space of [G_{inc}^{core},$G_{inc}^{rockfill}$] restricted to [10 kPa - 5000 kPa] , in order to get an idea about the location of probable solutions. Then, after the proper range of potential solutions was defined, the boundary was further limited to the range [2500 kPa - 4660 kPa] for the core and [10 kPa – 280 kPa] for the rockfill. Figure (3) presents the best solution set obtained. It can be concluded that the lowest error function value is $F_{err} = 1.50 \cdot 10^{-3}$ (m) which can be considered as the upper error function limit for case A.

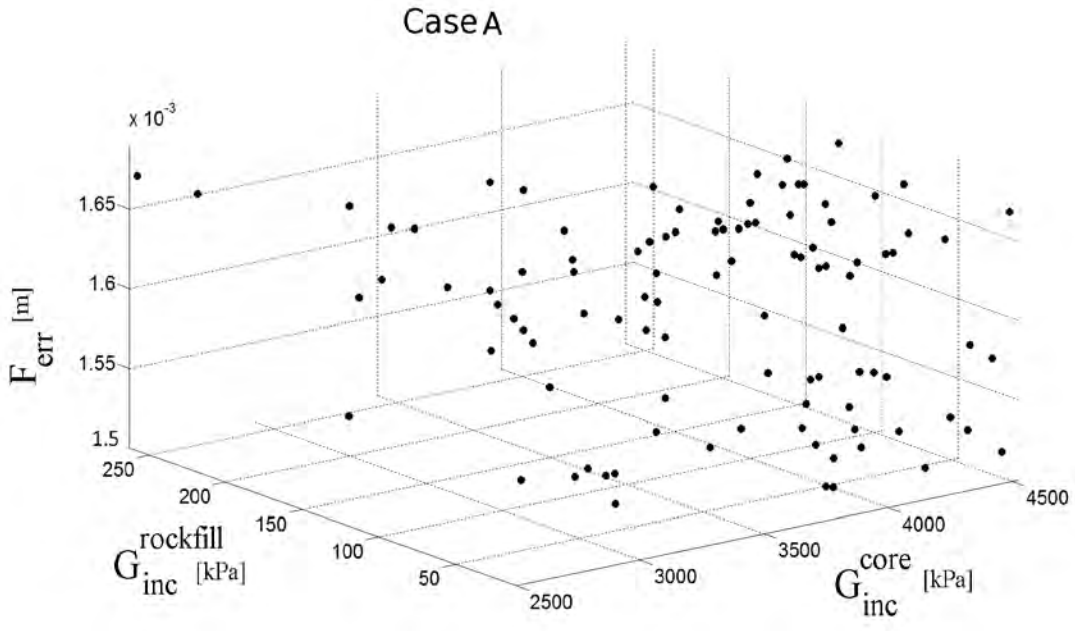

Figure 3: Best solution set for case A with the Mohr-Coulomb model

HARDENING SOIL MODEL

Before optimization, a sensitivity analysis of the model parameters in table (1) was utilized to characterize the influence of each parameter. From this, it was found that the reference secant stiffness of the core E_{50C}^{ref} and the reference secant stiffness of the rockfill E_{50R}^{ref} were two of the

most sensitive parameters for the horizontal deformation in the downstream zone of the dam. Therefore, these two parameters were chosen as the optimization variables in this study.

Ten inverse analyses were performed with the population size of 120 for the two cases A and B. In order to have a broad perspective about the location of the probable solution sets within the domain of [E_{50C}^{ref}, E_{50R}^{ref}], large limits [5 MPa-100 MPa] were chosen for E_{50C}^{ref} and E_{50R}^{ref}. The best error function value $F_{err} = 1.7 \cdot 10^{-2}$ (m) obtained from the previous study by Vahdati et.al (2013), is considered as an upper limit for the acceptable solutions for case B. For case A, as previously defined, an error function value of $F_{err} = 1.5 \cdot 10^{-3}$ (m) is considered as an upper limit for acceptable solutions. All the solutions which have an error function value less than the defined upper limit for each case, have the potential of being answers. In this research, each optimization parameter is encoded by 6 bytes in the genetic algorithm. Then the search domain consists of 2^6 times 2^6 nodes, 4906 discrete points with a mesh resolution of Δ1.48 MPa.

Figures (4) and (5), present the set of solutions below the upper limit of F_{err}, of ten inverse analyses for the cases A and B, respectively. One can conclude that for case A, the acceptable solutions for the value of E_{50R}^{ref} is limited to [13 MPa to 18 MPa], while this range is from [55 MPa-95 MPa] for E_{50C}^{ref}. On the other hand, for case B this range for E_{50R}^{ref} is limited to [10 MPa-20 MPa] and for E_{50C}^{ref} to [20 MPa-100 MPa]. Moreover, from these analyses it can be concluded that the horizontal deformation is more sensitive to the value of E_{50R}^{ref} than E_{50C}^{ref}, since the range of acceptable solutions became more limited for E_{50R}^{ref} than E_{50C}^{ref}. As can be seen in figures (4) and (5), the solutions differ with an integer multiple of 1.48 MPa, which is related to the mesh size chosen for the search domain.

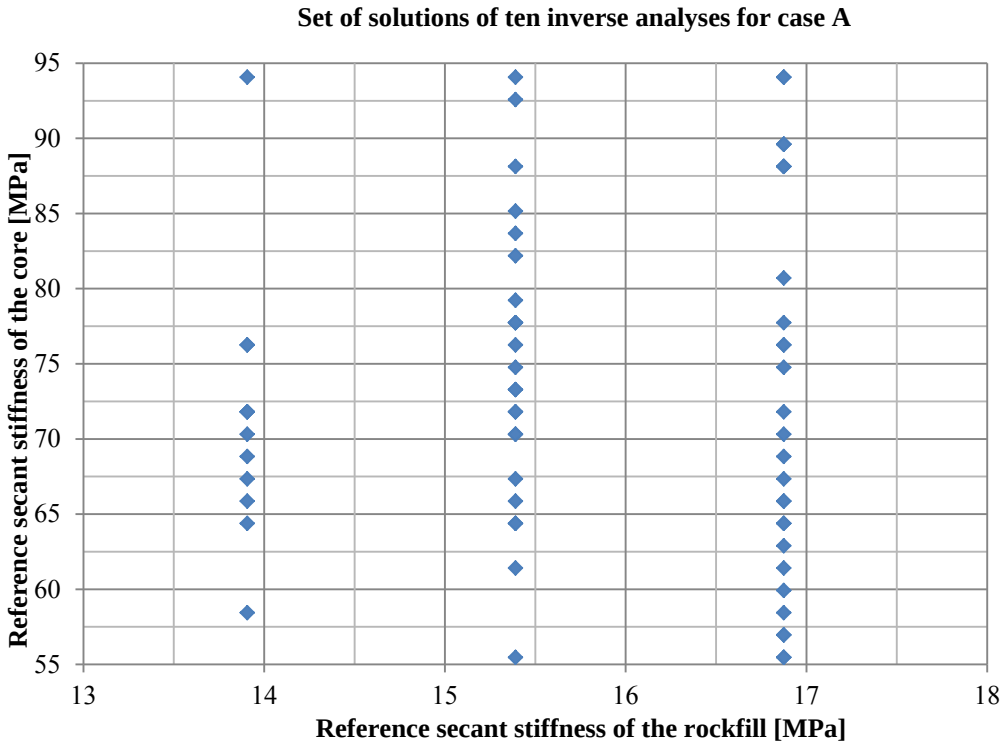

Figure 4: Set of solutions of ten inverse analyses for case A

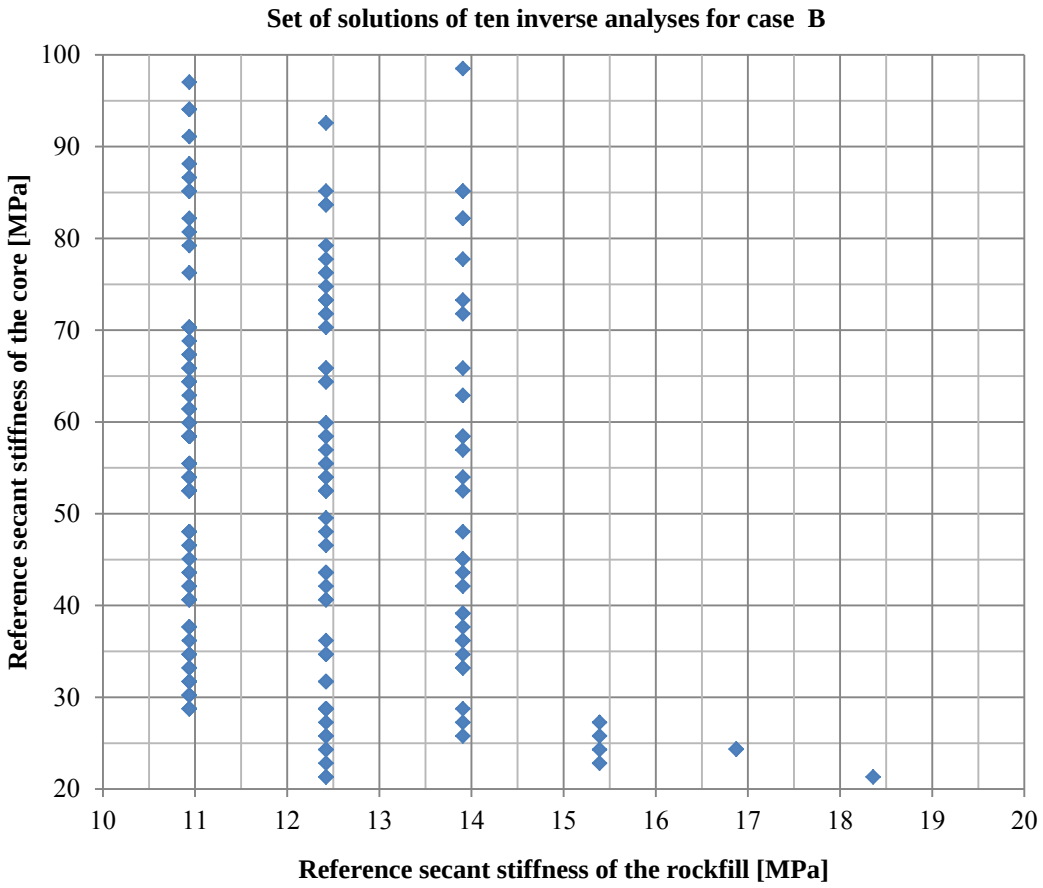

Figure 5: Set of solutions of ten inverse analyses for case B

Figure (6) presents the evaluation of the average error function value $\overline{F}_{err}$ versus the number of finite element computations for one chosen inverse analysis of cases A and B, respectively. This results show how the average error function value decrease when the set of solutions is gradually improved in the process of optimization. The process of optimization begins from a random initial population (240 computations) and continues until it converges to the best set of solutions. It can be seen, that for case A, the process converges after seven generations and 424 finite element computations to the value of $\overline{F}_{err} = 1.40 \cdot 10^{-3}$ (m) and for case B the process converges after six generations and 392 finite element computations to $\overline{F}_{err} = 1.29 \cdot 10^{-2}$ (m). Convergence is reached when the optimization process is no longer able to approach better results, then the average error function value gets more or less constant for each new generation of a new population, marked with square symbols in figure (6). The number of finite element computations is closely related to computation time.

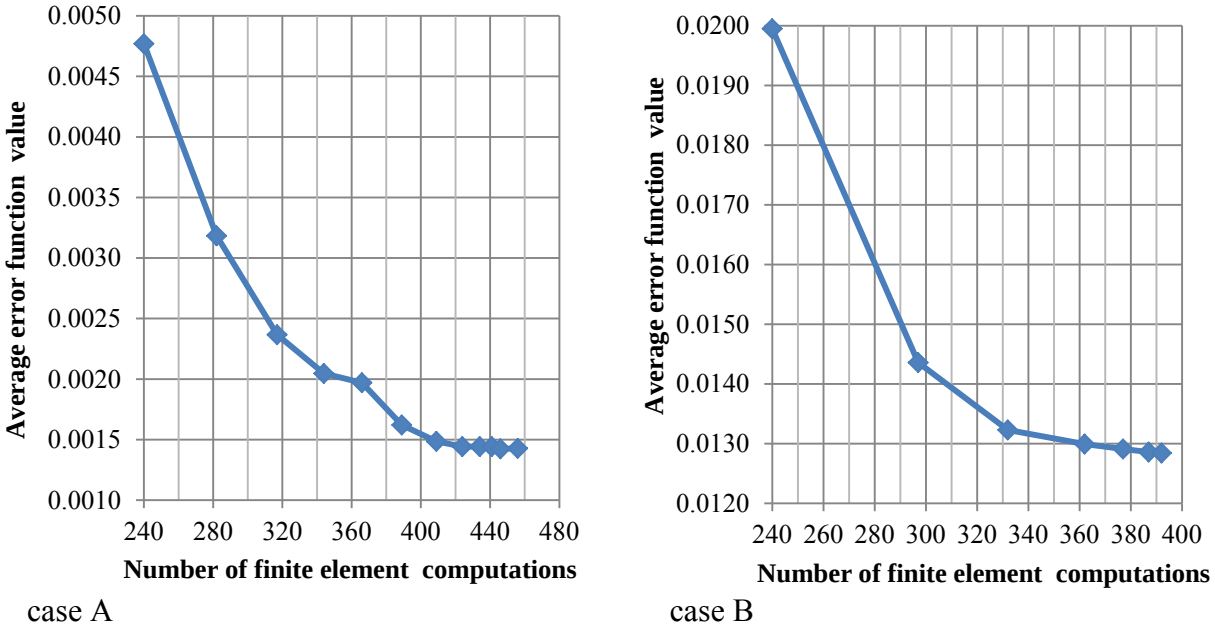

Figure 6: Average error function values versus number of finite element computations for the large search domain

STUDY OF ERROR FUNCTION TOPOLOGY

The purpose of this study is to find a graphical shape of the error function in order to monitor the smoothness properties of the surface and examine the location of the global optimum as well as the distribution of local optima in the search domain. Since only two optimization variables are involved, it is convenient to study the topology of the error function graphically in this case.

Figures (7) and (8) represent the topology and the level contours of the error function for case A and case B, respectively. The error function values F_{err} were plotted in the search domain limited to [5 MPa-100 MPa] for the optimization variables E_{50C}^{ref} and E_{50R}^{ref}. For both cases A and B, a distinct valley is visible on the error function surface in the low range of E_{50R}^{ref} values [10 MPa-20 MPa]. This valley that contained the location of the global optimum is extended with a slight inclination along the whole search range for E_{50C}^{ref} values [5 MPa-100 MPa]. The error function surface of case A has smaller fluctuations and noises with a number of local optima spread over the entire search domain, while the error function surface of case B is smooth. Therefore, the genetic algorithm is an appropriate choice for this application since the algorithm is not limited by smoothness properties of the error function and is not easily trapped into local optima.

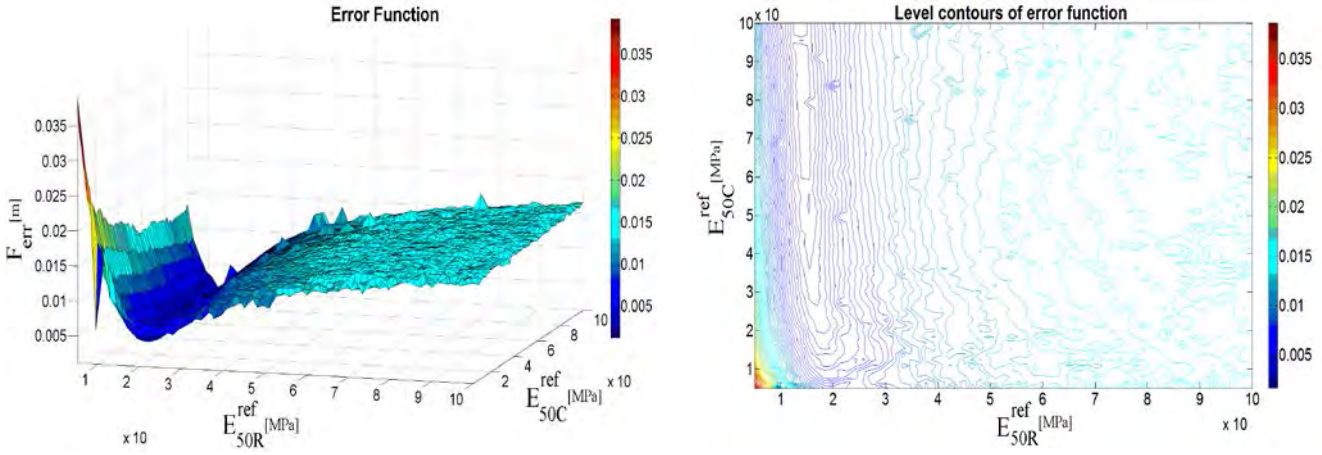

(a) (b)

Figure 7: Case A (a) error function topology (b) level contours of error function

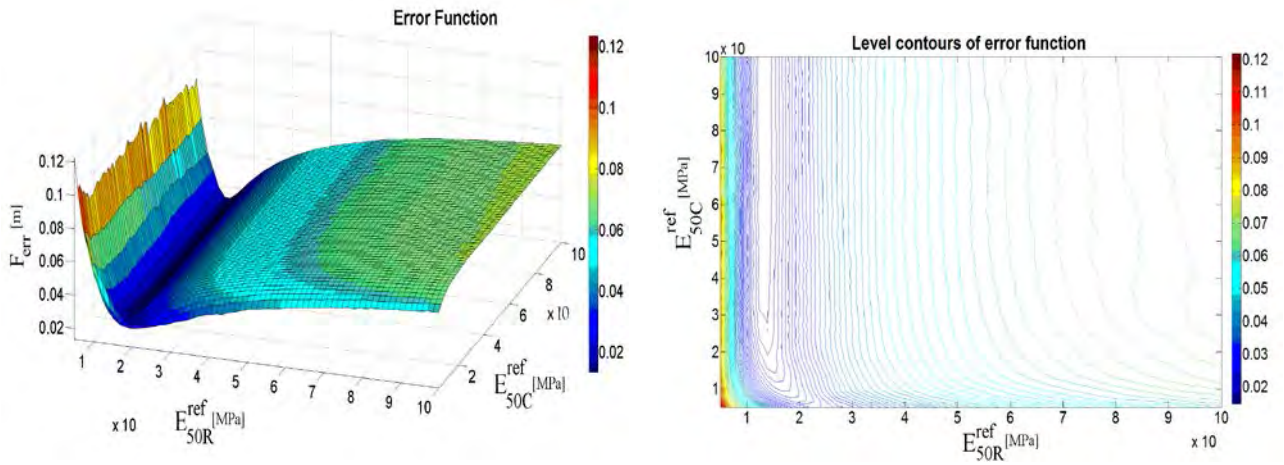

(a) (b)

Figure 8: Case B (a) error function topology (b) level contours of error function

INVERSE ANALYSIS WITH REDUCED SEARCH DOMAIN OF CASE A AND B

In order to improve the optimization search within the [E_{50R}^{ref} , E_{50C}^{ref}] space, the search domain is further limited to the range of the solution sets in figures (4) and (5). For case A, the search domain is limited to [13 MPa-18 MPa] for E_{50R}^{ref} and [55 MPa-95 MPa] for E_{50C}^{ref} with the mesh size of ΔE_{50R}^{ref} = 78.125 kPa and ΔE_{50C}^{ref} = 625 kPa, respectively. For case B, the search domain is limited to [10 MPa-20 MPa] for E_{50R}^{ref} and [20 MPa-100 MPa] for E_{50C}^{ref} with the mesh size of ΔE_{50R}^{ref} = 156.250 kPa and ΔE_{50C}^{ref} =1250 kPa, respectively. Since the mesh size of case B is twice

the mesh size of case A, it is easier to compare the set of solutions from case A and case B, with each other.

Another ten inverse analyses, limited to the reduced domain, were performed in order to find the best set of solutions for case A and B. Solutions are defined before as points with $F_{err} < 1.5 \cdot 10^{-3}$ (m) for case A and $F_{err} < 1.7 \cdot 10^{-2}$ (m) for case B and convergence is reached when $\overline{F}_{err}$ gets more or less constant in the optimization process.

Figure (9) presents the topologies of interpolated error function values of all solution points of the ten inverse analyses for both case A and case B within the reduced domain of [E_{50C}^{ref} , E_{50R}^{ref}]. For case A, there are two valleys in the defined domain area. The first one is located in the area of [75 MPa-100 MPa] for the E_{50C}^{ref} and [13.5 MPa-14.5 MPa] for the E_{50R}^{ref} and the second valley is located in the area of [70 MPa-100 MPa] for the E_{50C}^{ref} and [15.5 MPa-17 MPa] for the E_{50R}^{ref}. For case B, the best potential solutions are roughly located within the range of [20 MPa-100 MPa] for the E_{50C}^{ref} and [10.5 MPa-13 MPa] for the E_{50R}^{ref}.

In Figure 10 the blue rectangle as well as the blue parallelogram are defined as the areas of the best solutions of case A and the red rectangle is defined as the best solutions of case B. It can be seen that in case B the value of the rockfill stiffness is lower compared to case A. It is difficult to evaluate the best solution, representative of both case A and case B at the same time based on figure (10), but it feels like such a solution should be taken somewhere in the range [70 MPa- 100 MPa] for E_{50C}^{ref} and [10.5 MPa-17 MPa] for E_{50R}^{ref}. It is more likely that E_{50C}^{ref} has a constant value, common for both case A and B, than E_{50R}^{ref}. This is because the most probable solutions, representative for cases A and B, are located within the E_{50C}^{ref} range of [70 MPa- 100 MPa] and E_{50R}^{ref} range of [10.5 MPa-17 MPa]. This figure also shows that in case B the rockfill stiffness is lower compared to that in case A. However, in case A, the best solution gives the parameter values of E_{50C}^{ref} = 90 MPa and E_{50R}^{ref} = 14 MPa, with the error function value F_{err} = 0.0011 (m). For case B, the best solution becomes E_{50C}^{ref} = 90 MPa and E_{50R}^{ref} = 11 MPa with the error function value F_{err} = 0.0125 (m).

Figure 11 shows, for the best solution for case A and B respectively, the measured inclinometer values and the associated numerically simulated values of the horizontal displacement at different heights of the dam. The good agreement for both cases demonstrates that the Hardening soil model is able to simulate the trends of horizontal displacements. Moreover, the progress of the average error function value versus the number of finite element computations for one chosen inverse analysis for cases A and B were studied as well, see figure (12). For case A, the average error function value decreased step by step in the optimization and after 457 finite element computations and seven generations it converged to the value $\overline{F}_{err} = 1.16 \cdot 10^{-3}$ (m). For case B, after 284 finite element computations and five generations the average error function approached the value $\overline{F}_{err} = 1.25 \cdot 10^{-2}$ (m).

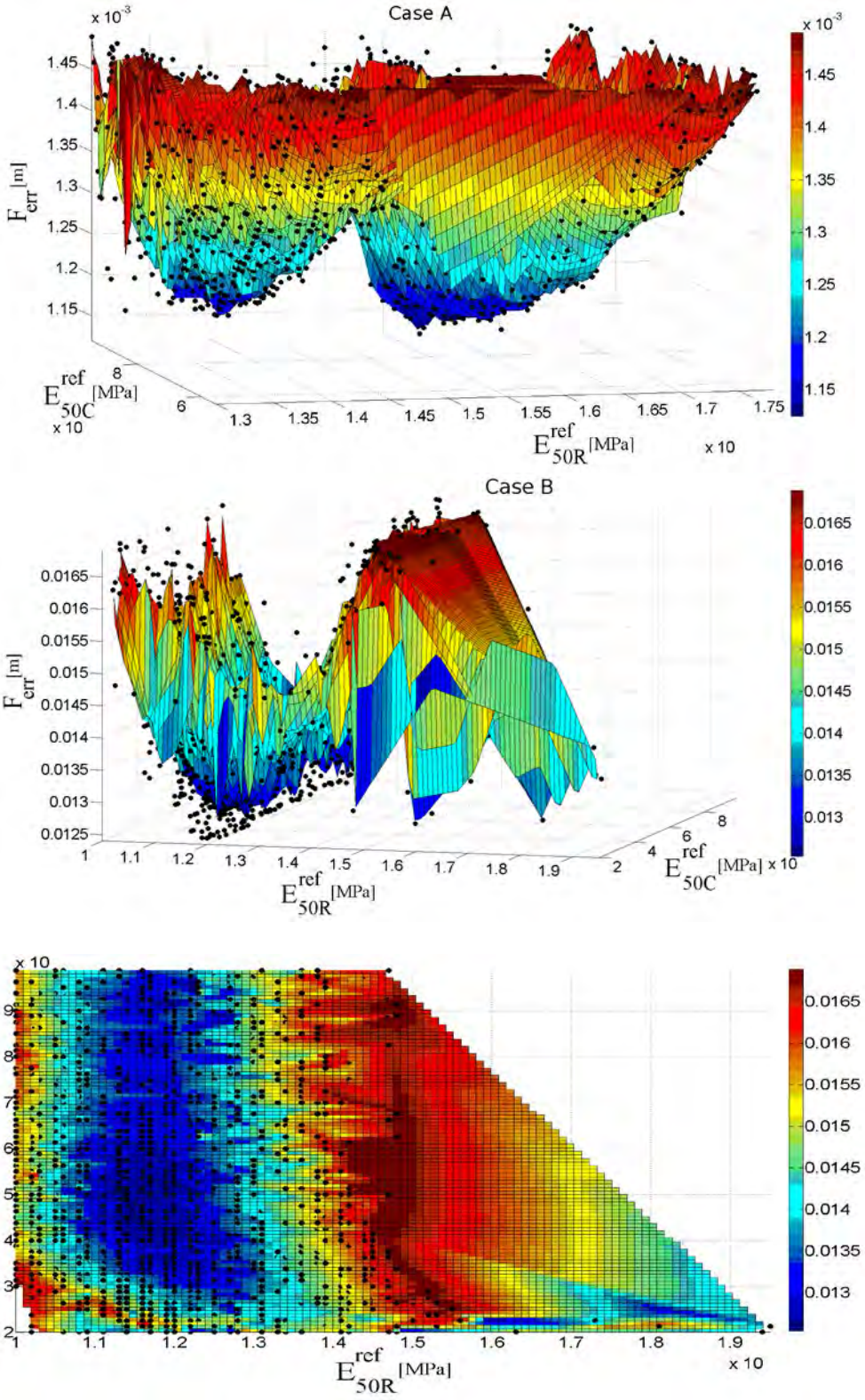
Case A
x 10^-3
F_err [m]
1.45
1.4
1.35
1.3
1.25
1.2
1.15
E_50C^ref [MPa]
x 10
8
6
1.3
1.35
1.4
1.45
1.5
1.55
1.6
1.65
1.7
1.75
E_50R^ref [MPa]
x 10
Case B
F_err [m]
0.0165
0.016
0.0155
0.015
0.0145
0.014
0.0135
0.013
0.0125
1
1.1
1.2
1.3
1.4
1.5
1.6
1.7
1.8
1.9
E_50R^ref [MPa]
2
4
6
8
E_50C^ref [MPa] x 10
x 10
E_50C^ref [MPa]
9
8
7
6
5
4
3
2
1
1.1
1.2
1.3
1.4
1.5
1.6
1.7
1.8
1.9
E_50R^ref [MPa]
x 10
0.0165
0.016
0.0155
0.015
0.0145
0.014
0.0135
0.013

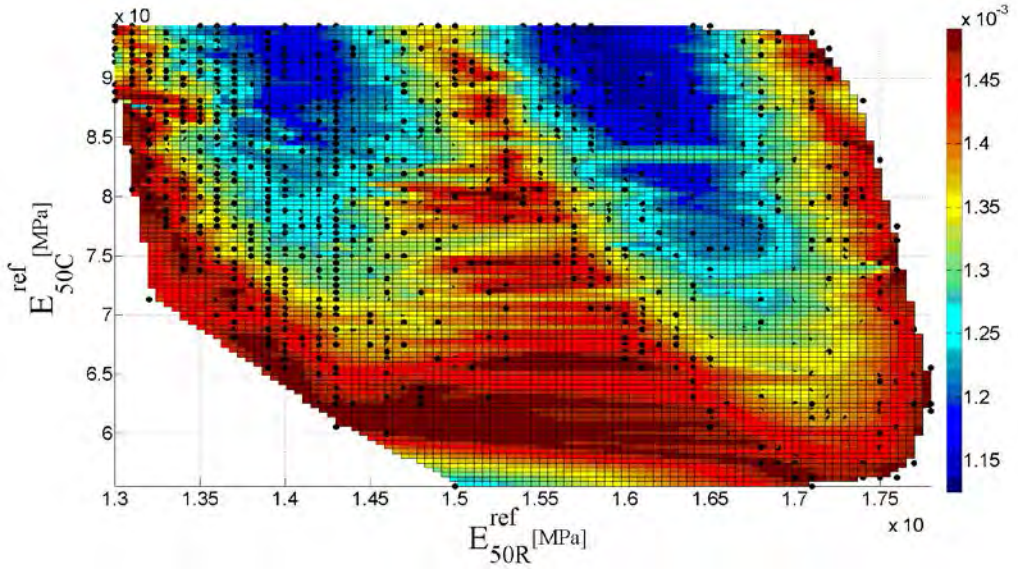

Figure 9: Best set of solutions in the domain of [E_{50C}, E_{50R}] for cases A and B

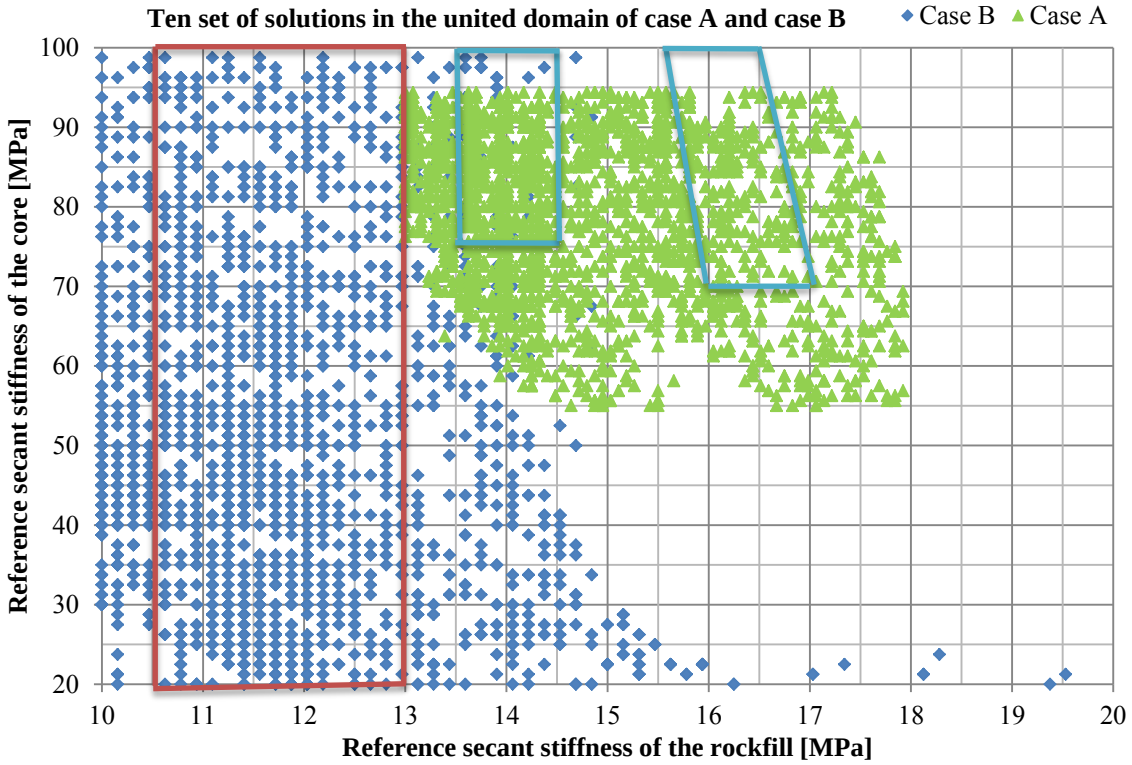

Figure 10: Set of solutions in the united domain [$E_{50C}^{ref}, E_{50R}^{ref}$] of cases A and B

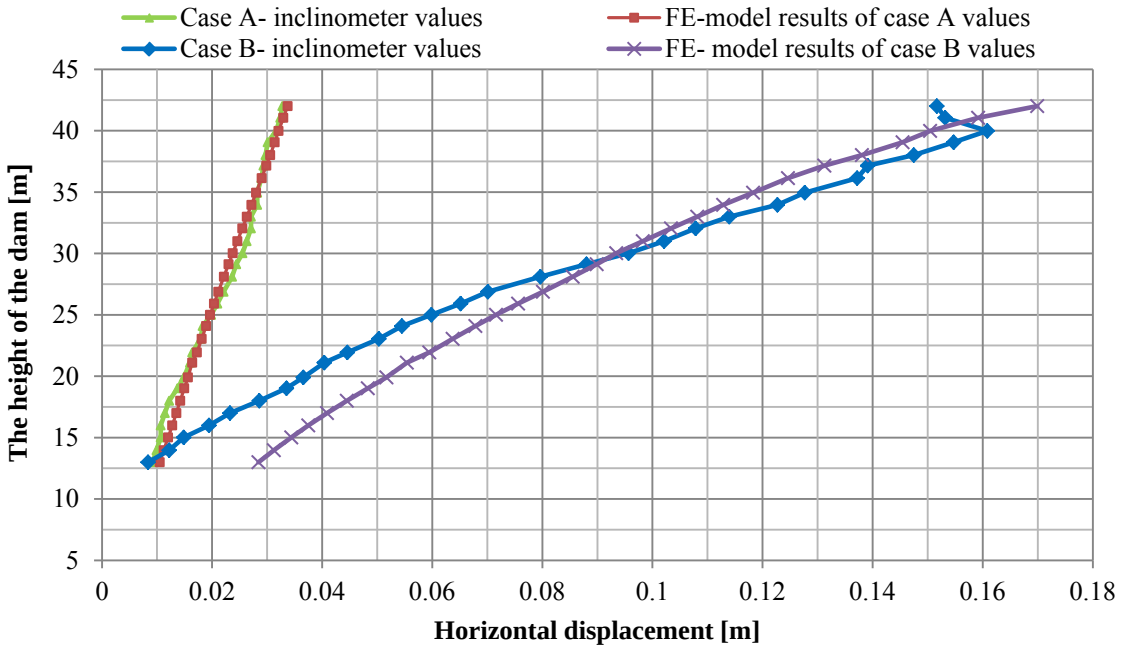

Figure 11: Measured and computed horizontal displacements at different heights of the dam for cases A and B

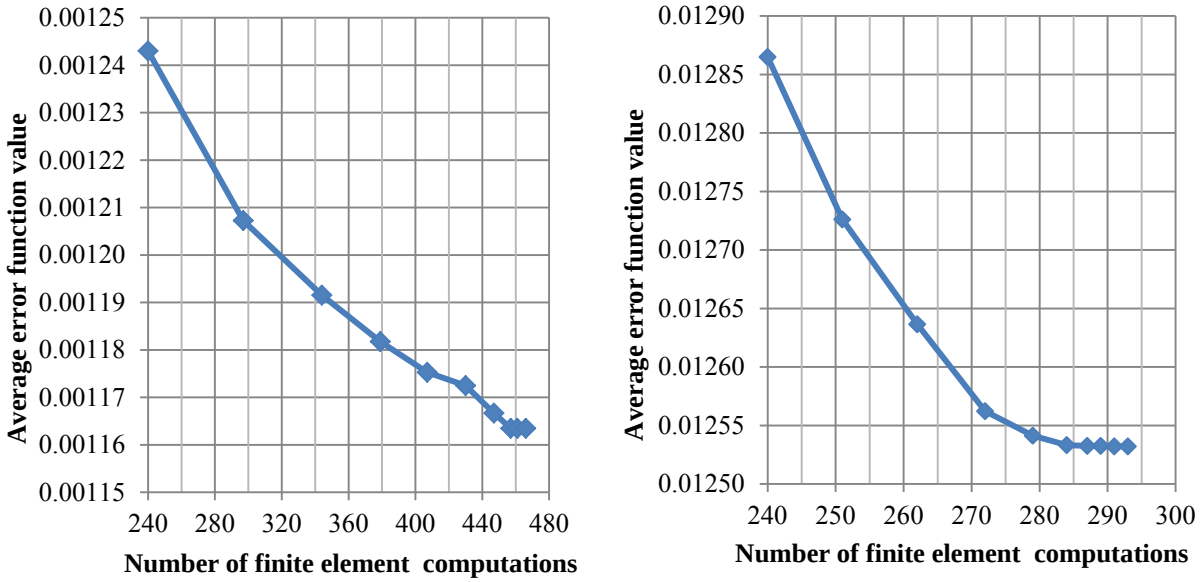

Case A Case B

Figure 12: Average error function values versus number of finite element computations for the reduced search domain

PLASTIC POINTS ON DIFFERENT YIELD LOCI IN THE HARDENING SOIL MODEL

One way of monitoring whether all mathematical parts of a constitutive model are active or not during numerical simulation, is to use the option *plastic points* in Plaxis. The plastic points

are the stress points in a plastic state, which can be displayed on a plot of the undeformed geometry in Plaxis.

Figure (13) shows all the plastic points in the dam structure at the final stress state of case B. Plastic points are presented by small triangle symbols that have different color, based on their location on the cone-cap yield loci of the Hardening soil model, see figure (14a). The blue triangle represents points on the cap, the green triangle shows friction hardening points on the cone, the brown triangle represents points on the cone-cap connection and the red triangle indicates that the stresses lie on the Mohr-Coulomb failure line. Tension cut-off points are also presented in figure (13), such points are only possible for soils with cohesion. In figure (14b), hardening behavior of the model is demonstrated during plastic loading.

As can be seen in figure (13), all mathematical parts of the Hardening soil model are active during the numerical simulation of the dam. A finding that further confirms that the Hardening soil model seems to be a good choice of constitutive model for the type of dam application studied.

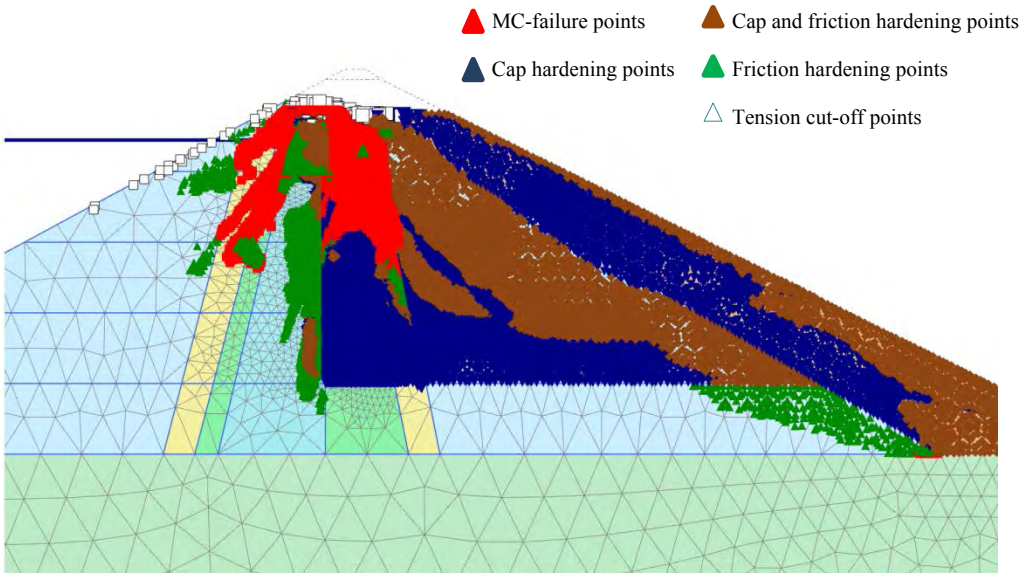

Figure 13: Plastic points on different yield loci

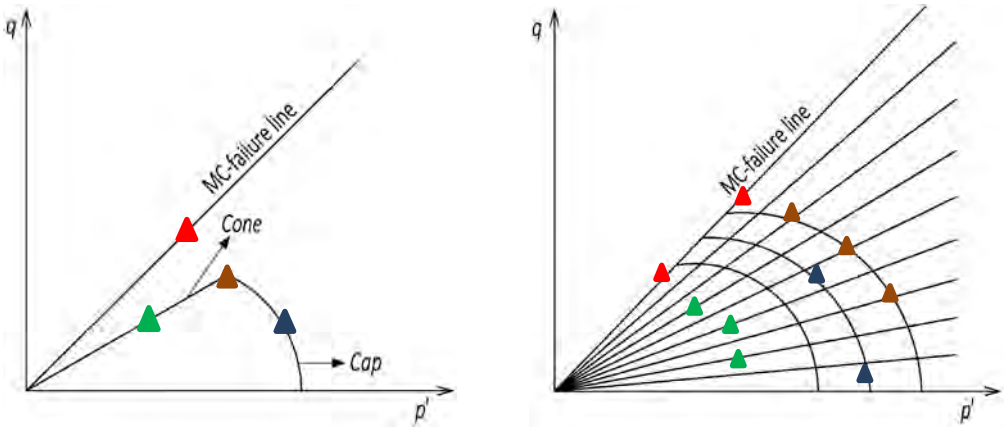

(a) (b)

Figure 14: Plastic points at Hardening soil model
(a) yield loci (b) multi hardened yield loci

CONCLUDING REMARKS

This research was focused on validating the technique of inverse analysis with the aim of identifying parameter values of constitutive models in an earth and rockfill dam application. The constitutive model chosen in this study was the Hardening soil model. The genetic algorithm was applied as the search method in the optimization.

Two case studies named A and B, regarding different reservoir water levels and numbers of berms constructed were considered for inverse analyses. Ten inverse analyses were performed for each case with the population size of 120 which was chosen based on a previous study by Vahdati et.al (2013). Initially, in order to have a broad perspective about the location of the probable solution set within the domain, large limits were chosen for the optimization variables. From these initial optimizations, a reduced search area was defined for cases A and B.

Thereafter, another ten inverse analyses were applied to each case in the reduced domain. Smaller mesh size in the search domain led to more solution points. Therefore, the probability of finding better solutions increased. The progress of the average error function value versus the number of finite element computations was studied for the ten inverse analyses in each case. It was seen that by reducing the search domain, better sets of solutions with lower error function values could be approached. A very good agreement for the simulation with the best solution was obtained against the inclinometer measurements for both case A and case B. The Hardening soil model captured the trend of horizontal displacements quite well.

The topology of the objective function for case A was found to be fluctuated while the surface for case B was found to be smooth without noticeable fluctuations. From this study and the previous study, Vahdati et.al (2013) can be concluded that the smoothness of the error function shape not only depends on the constitutive model chosen, smoothness depends also on the optimization case and the resolution in the search domain. Moreover, it can be concluded that the genetic algorithm is an appropriate option as search method for this rockfill dam application, since the genetic algorithm is not limited by smoothness properties of the error function surface and is not easily trapped into local optima. Many other types of search methods, like e.g. gradient and direct search methods, can be expected to face problems with the error function topology in this application.

In this research, two optimization variables were considered. An increased number of optimization variables will be considered for future work.

ACKNOWLEDGEMENTS

The research presented in this paper was carried out as a part of "Swedish Hydropower Centre - SVC". SVC has been established by the Swedish Energy Agency, Elforsk and Svenska Kraftnät together with Luleå University of Technology, The Royal Institute of Technology, Chalmers University of Technology and Uppsala University.

Participating hydro power companies are: Andritz Hydro Inepar Sweden, Andritz Waplans, E.ON Vattenkraft Sverige, Fortum Generation, Holmen Energi, Jämtkraft, Karlstads Energi, Linde Energi, Mälarenergi, Skellefteå Kraft, Sollefteåforsens, Statkraft Sverige, Statoil Lubricants, Sweco Infrastructure, Sweco Energuide, SveMin, Umeå Energi, Vattenfall Research and Development, Vattenfall Vattenkraft AB, VG Power and WSP.

REFERENCES

1. Bowles, J.E. (1988) "Foundation Analysis and Design". MacGraw-Hill. Berkshire. England.
2. Calvello, M. and Finno, R. (2002) "Calibration of soil models by inverse analysis". Numerical Models in Geomechanics NUMOG VIII, pp. 107-116.
3. Calvello, M. and Finno, R.J. (2004) "Selecting Parameters to Optimize in Model Calibration by Inverse Analysis". Computers and Geotechnics, vol. 31, no. 5, pp. 410-424.
4. Carroll, D.L. (1996) "Genetic algorithms and optimizing chemical oxygen-iodine lasers". Developments in Theoretical and Applied Mechanics, vol. 18, no. 3, pp. 411-424.
5. Chelouah, R. and Siarry, P. (2000) "A continuous genetic algorithm designed for the global optimization of multimodal functions". Journal of Heuristics, vol. 6, no. 2, pp. 191-213.
6. Clough, R.W. and Woodward, R.J. (1967) "Analysis of Embankment Stresses and Deformations". Journal of Soil Mechanics & Foundations Div. Vol 93, pp. 529-549.
7. Duncan, J.M. and Chang, C.Y. (1970) "Nonlinear analysis of stress and strain in soils". Journal of the Soil Mechanics and Foundations Division, vol. 96, no. 5, pp. 1629-1653.
8. Duncan, J.M. (1981) "Hyperbolic Stress-Strain Relationships". Application of Plasticity and Generalized Stress-Strain in Geotechnical Engineering.
9. Duncan, J.M. (1996) "State of the Art: Limit Equilibrium and Finite-Element Analysis of Slopes". Journal of Geotechnical Engineering, vol. 122, no. 7, pp. 577-596.
10. Finno, R.J. and Calvello, M. (2005) "Supported Excavations: Observational Method and Inverse Modelling". Journal of Geotechnical and Geoenvironmental Engineering, vol. 131, no. 7, pp. 826-836.
11. Gallagher, K., Sambridge, M.S. and Drijkoningen, G. (1991) "Genetic Algorithms-an Evolution from Monte-Carlo Methods for Strongly Non-Linear Geophysical Optimization Problems". Geophysical Research Letters, vol. 18, no. 12, pp. 2177-2180.

12. Gioda, G. and Maier, G. (1980) "Direct Search Solution of an Inverse Problem in Elastoplasticity: Identification of Cohesion, Friction Angle and in Situ Stress by Pressure Tunnel Tests". International Journal for Numerical Methods in Engineering, vol. 15, no. 12, pp. 1823-1848.

13. Gioda, G. and Sakurai, S. (1987) "Back Analysis Procedures for the Interpretation of Field Measurements in Geomechanics". International Journal for Numerical and Analytical Methods in Geomechanics, vol. 11, no. 6, pp. 555-583.

14. Goldberg, D.E. (1989) "Genetic algorithms in search, optimization, and machine learning". Machine learning 3.2 (1988): 95-99

15. Goldberg, D.E., Deb, K. and Clark, J.H. (1991) "Genetic algorithms, noise, and the sizing of populations". Complex Systems, vol. 6, pp. 333-362.

16. Haupt, R.L. and Haupt, S.E. (2004) "Practical Genetic Algorithms". Wiley Online Library. New York.

17. Holland, J.H. (1975) "Adaptation in Natural and Artificial Systems". University of Michigan Press: MIT press: Ann Arbor.

18. Hunter, G. and Fell, R., 2003. The deformation behaviour of embankment dams. Uniciv report No. R-416. The University of New Wales, School of Civil and Environmental Engineering.

19. Kovacevic, N. (1994) "Numerical Analyses of Rockfill Dams, Cut Slopes and Road Embankments". PhD Thesis, London University (Imperial College of Science and Medicine), Faculty of Engineering.

20. Lecampion, B. and Constantinescu, A. (2005) "Sensitivity Analysis for Parameter Identification in quasi-static Poroelasticity". International Journal for Numerical and Analytical Methods in Geomechanics, vol. 29, no. 2, pp. 163-185.

21. Lecampion, B., Constantinescu, A. and Nguyen Minh, D. (2002) "Parameter Identification for Lined Tunnels in a Viscoplastic Medium". International Journal for Numerical and Analytical Methods in Geomechanics, vol. 26, no. 12, pp. 1191-1211.

22. Ledesma, A., Gens, A. and Alonso, E. (1996) "Estimation of Parameters in Geotechnical back analysis—I. Maximum Likelihood Approach". Computers and Geotechnics, vol. 18, no. 1, pp. 1-27.

23. Levasseur, S., Malecot, Y., Boulon, M. and Flavigny, E. (2009) "Statistical Inverse Analysis Based on Genetic Algorithm and Principal Component Analysis: Method and Developments using Synthetic Data". International Journal for Numerical and Analytical Methods in Geomechanics, vol. 33, no. 12, pp. 1485-1511.

24. Levasseur, S., Malecot, Y., Boulon, M. and Flavigny, E. (2008) "Soil Parameter Identification using a Genetic Algorithm". International Journal for Numerical and Analytical Methods in Geomechanics, vol. 32, no. 2, pp. 189-213.

25. Levasseur, S., Malecot, Y., Boulon, M. and Flavigny, E. (2010) "Statistical Inverse Analysis Based on Genetic Algorithm and Principal Component Analysis: Applications to Excavation Problems and Pressuremeter Tests". International Journal for Numerical and Analytical Methods in Geomechanics, vol. 34, no. 5, pp. 471-491.

26. Moreira, N., Miranda, T., Pinheiro, M., Fernandes, P., Dias, D., Costa, L., Sena-Cruz, J. (2013) "Back analysis of geomechanical parameters in underground works using an

Evolution Strategy algorithm". Tunnelling and Underground Space Technology. vol. 33, pp.143-158, Elsevier

27. Pal, S., Wije Wathugala, G. and Kundu, S. (1996) "Calibration of a Constitutive Model using Genetic Algorithms". Computers and Geotechnics, vol. 19, no. 4, pp. 325-348.
28. Papon, A., Riou, Y., Dano, C. and Hicher, P. (2012) "Single- and multi-objective genetic algorithm optimization for identifying soil parameters. International Journal for Numerical and Analytical Methods in Geomechanics, vol. 36, no. 5, pp. 597-618.
29. Plaxis. (2011) Finite Element Code for Soil and Rock Analysis. version 2011-2. http://plaxis.nl
30. Rechea, C., Levassur, S. and Finno, R. (2008) "Inverse Analysis Techniques for Parameter Identification in Simulation of Excavation Support Systems". Computers and Geotechnics, vol. 35, no. 3, pp. 331-345.
31. Resendiz, D. and. Romo, M.P (1972) "Analysis of embankment deformations". Anonymous Performance of Earth and Earth-Supported Structures. ASCE. Vol.1. pp. 817-836.
32. Rowe, P.W., 1962. "The stress-dilatancy relation for static equilibrium of an assembly of particles in contact". Proceedings of the Royal Society of London. Series A. Mathematical and Physical Sciences, vol. 269, no. 1339, pp. 500-527.
33. Schanz, T. and Vermeer, P. (1998) "On the stiffness of sands". Géotechnique, vol. 48, pp. 383-387.
34. Schanz, T., Vermeer, P., and Bonnier, P. (1999) "The hardening soil model: formulation and verification". Beyond 2000 in computational geotechnics: 10 years of PLAXIS International; proceedings of the International Symposium beyond 2000 in Computational Geotechnics, Amsterdam, The Netherlands, 18-20 March 1999.
35. Swoboda, G., Ichikawa, Y., Dong, Q. and Zaki, M. (1999) "Back Analysis of Large Geotechnical Models". International Journal for Numerical and Analytical Methods in Geomechanics, vol. 23, no. 13, pp. 1455-1472.
36. Tarantola, A. (1987) "Inverse Problem Theory". Elsevier. Amsterdam.
37. Vahdati, P., Levasseur, S., Mattsson, H. and Knutsson, S. (2013) "Inverse Mohr-Coulomb soil parameter identification of an earth and rockfill dam by genetic algorithm optimization". Electronic Journal of Geotechnical Engineering, vol. 18, pp. 5419-5440.
38. Yu, Y., Zhang, B. and Yuan, H. (2007) "An Intelligent Displacement Back-Analysis Method for Earth-Rockfill Dams". Computers and Geotechnics, vol. 34, no. 6, pp. 423-434.
39. Zentar, R., Hicher, P. and Moulin, G. (2001) "Identification of Soil Parameters by Inverse Analysis". Computers and Geotechnics, vol. 28, no. 2, pp. 129-144.